

Development of an Aluminum Brazing Sheet Product with Barrier Layer for High-Performance Automotive Heat Exchangers



H. JIN

A high-strength aluminum brazing sheet product has been developed for automotive heat exchangers. It consists of commercial Al-Si clad, newly designed Al-Mn-Cu-Mg core, and pure aluminum barrier between the clad and core. The microstructure, mechanical properties, corrosion resistance, and braze-ability were investigated and compared with regular brazing sheets without barrier. The newly designed Al-Mn-Cu-Mg alloys are much stronger than commercial Al-Mn-Cu core alloys and the high strength is maintained up to 573.15 K (300 °C). However, liquid–solid interaction occurs extensively during brazing when the Al-Si clad contacts the Al-Mn-Cu-Mg core directly, resulting in degrading of mechanical properties and corrosion resistance. The barrier provides a physical separation between the clad and core, preventing not only the liquid–solid interaction, but also the solid diffusion of Si from clad to core and Mg from core to sheet surface. The accumulation of Si and Mg in the barrier leads to a high population density of Mg₂Si precipitates, acting as a sacrificial band to delay the through-thickness corrosion. Meanwhile, the low Mg level in the sheet surface ensures high braze-ability for commercial flux brazing processes. The new sheet product is therefore suitable to high-performance automotive heat exchangers, especially the ones that may serve at temperatures above 473.15 K (200 °C).

<https://doi.org/10.1007/s11661-021-06172-1>
© Crown 2021

I. INTRODUCTION

ALUMINUM brazing sheets have been used to make automotive heat exchangers for decades. Most of them are 2 or 3-layered composites with a core, ~ 80-90 pct of sheet thickness, covered by clad, ~ 10 to 20 pct of sheet thickness, in one or both sides.^[1–4] The core is usually made of AA3xxx alloys with high Mn and Cu, 1.2 to 1.5 pct and 0.5 to 0.7 pct, respectively, and low Mg and Si, < 0.5 pct and < 0.2 pct, respectively (all in wt. hereinafter). The clad is made of AA4xxx Al-Si filler alloys at or below the eutectic point, *i.e.*, ≤ 12.7 pct Si, with melting temperature at ~ 850.15 K (577 °C). In commercial brazing processes, *e.g.*, Alcan NOCOLOK™ flux brazing, the fin-and-tube assembly of heat exchanger is heated up quickly to ~ 873.15 K (600 °C) in continuous heating line and followed by relatively quick cooling to room temperature.^[5] The clad melts during the heating-up stage and re-solidifies upon cooling-down, making the fin-and-tube welded together.

Ideally, in the whole process, the core should remain solid, and after brazing, it should have desired strength and corrosion resistance within service temperature range.^[6,7]

The maximum service temperature of conventional automotive heat exchangers is 393.15 K to 423.15 K (120 °C to 150 °C).^[8,9] This limitation is due to the softening of aluminum alloys at elevated temperatures. For example, commercial Alcan X901 Al-1.5 pct Mn-0.5 pctCu core alloy has post-braze yield strength (YS) at ~ 65 MPa below 473.15 K (200 °C), but the strength drops quickly at higher temperatures, *e.g.*, ~ 55 MPa at 523.15 K (250 °C) and ~ 40 MPa at 573.15 K (300 °C).^[6,7] Meanwhile, many high-performance automotive heat exchangers are beneficial of higher service temperatures. For instance, the capacity of modern super/turbo-charger technologies is often limited by the maximum allowable operating temperature of charge air coolers. If the charge air coolers could endure higher operating temperatures, *e.g.*, 473.15 K to 573.15 K (200 °C to 300 °C), significant increase of boost and fuel economy could be achieved.^[10,11] Therefore, there is a demand of new brazing sheet products capable of maintaining high strength at above 473.15 K (200 °C). Such products are also beneficial to the heat exchangers used in low temperature range, since high

H. JIN is with the CanmetMATERIALS, Natural Resources Canada, Hamilton, ON L8P 0A5, Canada. Contact e-mail: haiou.jin@canada.ca

Manuscript submitted 20 October 2020; accepted 29 January 2021.
Article published online February 20, 2021

strength enables decrease of sheet thickness, leading to weight reduction and better heat exchange efficiency.

In a previous work, 0.5-2 pct Mg was added to Alcan X901 core alloy.^[7,12] It was found that the Mg improves the strength significantly up to 573.15 K (300 °C) by solid solution and grain boundary hardening. However, the Mg meanwhile reduces the melting point and grain size, raising a concern of reduction of corrosion resistance by grain boundary penetration (GBP). The GBP, where liquid Al-Si penetrates deeply into the core along grain boundaries, is very detrimental and may result in significant changes of local chemistry and microstructure.^[13-16] To prevent the GBP, in the present work, a pure aluminum barrier layer was added between the clad and core. Its effects on microstructure and mechanical properties were systematically investigated, in comparison with regular brazing sheets without barrier layer. The theoretical assessment of corrosion resistance and braze-ability will be discussed briefly, but the experimental part is to be reported elsewhere. It was intended to develop a new aluminum brazing sheet product that tolerates higher service temperature without reducing the corrosion resistance or braze-ability for high-performance automotive heat exchangers, especially the ones associated with super/turbo-charged engines.

II. EXPERIMENTS

Five aluminum alloys were involved: AA4045 for the clad, AA1100 for the barrier layer, and three Al-Mn-Cu-Mg alloys for the core. While a 2.54 mm commercial AA1100 H14 sheet was used as the starting material for the barrier, the clad and core alloys were fabricated in the lab. Four 610 mm × 229 mm × 95 mm ingots were cast by direct chill (DC) casting: one was AA4045 Al-10 pctSi clad alloy, and the others were Al-1.5 pctMn-0.5 pctCu core alloys with 1, 1.5 and 2 pct Mg labeled by Alloys-A, B, and C, respectively. The chemical compositions of the five alloys are listed in Table I. All the ingots were scalped by ~ 10 mm from each rolling face to remove the shell zone. The AA4045 ingot was re-heated to ~ 793.15 K (520 °C), hot rolled to ~ 8 mm, and then cold rolled to ~ 2.2 mm, while the Al-Mn-Cu-Mg ingots were re-heated to ~ 793.15 K (520 °C) and hot rolled to ~ 18 mm.

Table I. The Chemical Compositions of the Clad, Barrier and Core Alloys, as Well as the X901 in Commercial AA4045-X901 H24 Brazing Sheet, all in Wt Pct, Determined by Inductively Coupled Plasma-Optical Emission Spectrometry

Alloy	Mn	Cu	Mg	Fe	Si	Ti	Al
AA4045	—	—	—	0.14	9.88	0.02	balance
AA1100	0.06	0.05	—	0.55	0.15	0.01	balance
Alloy-A	1.48	0.54	1.00	0.26	0.11	0.01	balance
Alloy-B	1.52	0.54	1.52	0.24	0.11	0.01	balance
Alloy-C	1.52	0.55	1.95	0.24	0.10	0.02	balance
X901	1.52	0.50	0.11	0.24	0.09	0.01	balance

A total of six brazing sheets were made in two sets: Sheets I, II, and III with barrier layer and Sheets 1, 2, and 3 without barrier layer. For the first set, the AA4045, AA1100, and Al-Mn-Cu-Mg plates were welded in the feeding edge to make single-side clad-barrier-core assemblies. The assemblies were re-heated to 723.15 K (450 °C), roll-bonded to ~ 5 mm by hot rolling, and cold rolled down to ~ 1 mm. To match the popular as-supplied condition of commercial products, the as-rolled sheets were batch annealed at 560.15 K (287 °C) for 2 hours to reach the H24 temper. These sheets were designated as Sheets I, II, and III corresponding to the core alloys of A, B, and C, respectively. For the second set, the thermo-mechanical processing is identical to the first set but without the barrier plate. These sheets were designated as Sheets 1, 2, and 3 corresponding to A, B, and C core alloys, respectively. In addition, a 1-mm single-side clad commercial AA4045-X901 H24 long-life brazing sheet, designated as Sheet control, was used for comparison. The clad is 10 pct of the sheet thickness, and the chemistry of X901 is listed in Table I.

Tensile specimens with 12.7 mm gauge width and 19.1 mm gauge length were machined along the rolling direction (RD). To roughly simulate the heating cycle of NOCOLOK™ flux brazing, the specimens were flash annealed through a belt furnace: quick heating to ~ 873.15 K (600 °C), soaking for ~ 3 minutes and followed by fast air cooling (Figure 1). The specimens were laid on the belt with the clad side upwards so the molten Al-Si stayed on the surface without dripping off, which is the most severe condition for liquid-solid interaction. Afterwards, the specimens were further treated to reach the W, T4 and T6 tempers. The W temper refers to the condition within 15 minutes after flash annealing, *i.e.*, the testing must be done within 15 minutes, the T4, flash annealed and stored at room temperature for half year, and the T6, flash annealed, stored at room temperature for half year, and followed by artificial aging at 453.15 K (180 °C) for 8 hours. Tensile testing was done in an Instron 6040 machine with a constant cross-head speed equivalent to 6×10^{-4} s⁻¹ strain rate in a heating chamber. While the specimens in W temper were tested at room temperature only, the ones in T4 and T6 tempers, at room temperature and 373.15 K, 423.15 K, 473.15 K, 523.15 K, 573.15 K, and 618.15 K (100 °C, 150 °C, 200 °C,

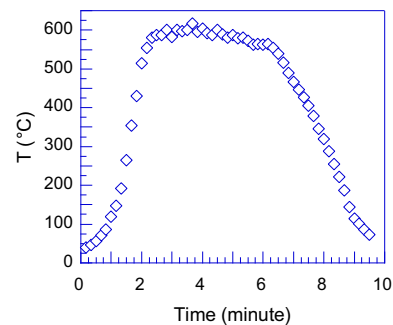


Fig. 1—The temperature–time profile of simulated brazing cycle.

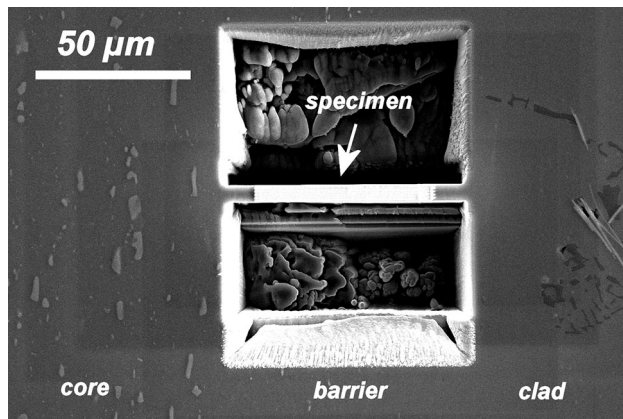


Fig. 2—Preparation of TEM specimen by FIB lift-out technique in a brazing sheet with barrier layer. The RD is vertical and the thickness direction is horizontal.

250 °C, 300 °C, and 345 °C). For the testing at elevated temperatures, the chamber was pre-heated and it took ~ 15 minutes for the specimen to reach the testing temperature. Three specimens were tested for each condition and the average values of YS, ultimate tensile strength (UTS), and fracture elongation (EL) were recorded.

The microstructure was examined by Olympus PMG3 optical microscope, Philips XL30 scanning electron microscope (SEM), and FEI Tecnai Osiris transmission electron microscope (TEM). While the grain size was determined by line intercept method on SEM electron backscatter images, the phase identification was done by energy dispersive X-ray (EDX) analysis in SEM and TEM, as well as selected area diffraction analysis in TEM. The solid-state diffusion of Mg, Si, Mn, and Cu was evaluated by SEM-EDX line scanning in the thickness direction. All the metallographic specimens were prepared by mechanical polishing in the longitudinal section, defined by the RD and thickness direction, with diamond pastes down to 1 μm followed by mechanical-chemical polishing using 0.5 μm colloidal silica. To reveal the intermetallic particles clearly, the specimens for optical microscopy were etched in 0.5 pct HF water solution for 15 seconds. The TEM specimens were prepared in the T4 and T6 tempers by lift-out technique in FEI Helios NanoLab 650 focus ion-beam (FIB) microscope. For Sheets I, II, and III, the TEM specimens were made in the barrier layer, as shown in Figure 2. For Sheets 1, 2, and 3 without barrier layer, the specimens were made in the core side immediately adjacent to the clad.

III. RESULTS

A. Microstructure Before Brazing

The longitudinal section of the as-rolled sheets with barrier layer is shown in Figure 3. The clad and barrier have nearly the same thickness, ~ 100 μm, equivalent to 10 pct of the total thickness, with clear and straight interfaces. For the as-rolled sheets without barrier layer,

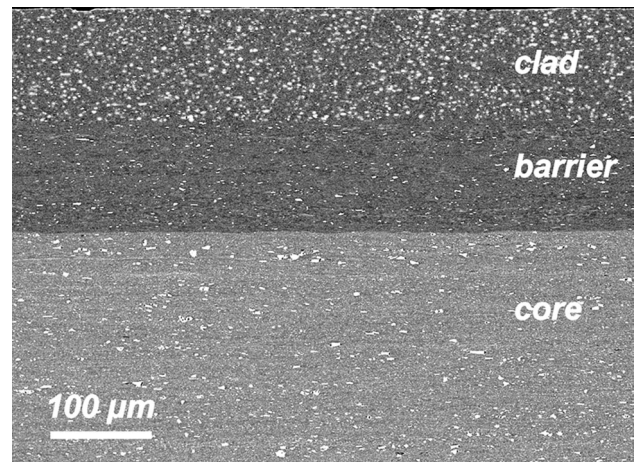


Fig. 3—SEM backscatter image of as-rolled Sheet III. The RD is horizontal and the thickness direction is vertical.

the clad is also 10 pct of the thickness and the interface is clear and straight as well. Figure 4 shows the microstructure of H24 temper. The clad and barrier are fully recrystallized with relatively equi-axed grain structure, but the core is only partially recrystallized. The lightly deformed structure in AA1100 barrier layer shown in Figure 4(a) is not residual rolling structure; instead, it was generated artificially during specimen polishing, as the fully annealed AA1100 is extremely soft. The mean grain sizes in the clad and barrier are ~ 5 and ~ 75 μm, respectively.

Figure 5 shows the secondary phase particles in H24 sheets. The clad contains evenly distributed Si particles with spherical/oval shape and 1 to 5 μm size, as well as spherical Al-Fe-Si intermetallic particles below 1 μm (Figure 5(a)). A limited number of Al-Fe and Al-Fe-Si intermetallic particles were found in the barrier, having different sizes from below 1 to ~ 10 μm (Figure 5(b)). In the core, the intermetallic particles are nearly all of the Al₆(Mn,Fe) phase, either coarse constituents from several to several ten micrometers or relatively fine dispersoids below 1 μm (Figure 5(c)). The sizes, volume fractions, and spatial distributions of the intermetallic particles in different core alloys are very similar, regardless of the different Mg levels. In addition, a few Al₂Cu and Mg₂Si dispersoid particles below 1 μm were also detected in the core. A report of detailed TEM analysis of the clad and core alloys could be found in Reference 7.

B. Microstructure After Brazing

After the simulated brazing cycle, the clad side surface of Sheets control, I, II, and III remained light gray, while that of Sheets 1, 2, and 3 appeared much darker. The appearance of dark gray is an indication of extensive surface oxidation of Mg. In Sheets I, II, and III, the re-solidified clad has a typical as-cast dendritic structure with primary aluminum and Al-Si eutectic (Figure 6). The barrier is little changed, except the mean grain size has been coarsened to ~ 100 μm. The core is fully recrystallized and the grain structure becomes finer

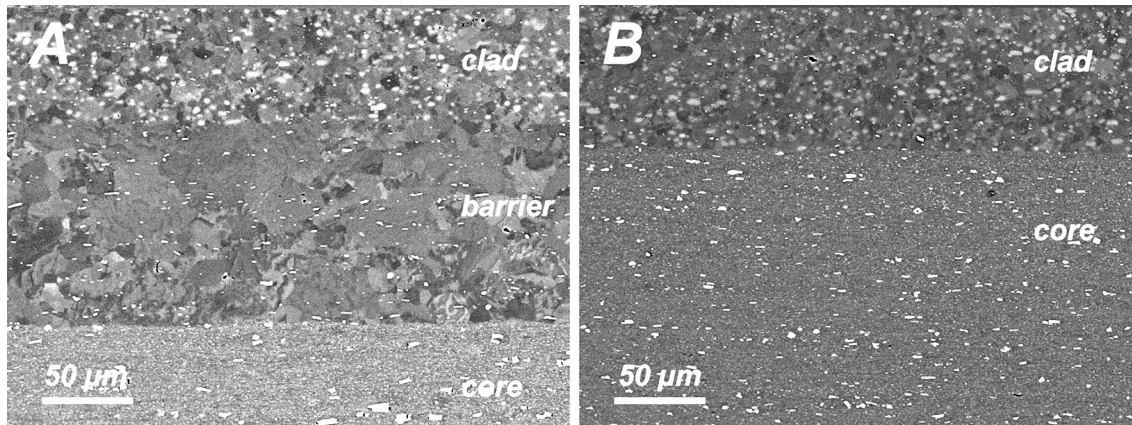


Fig. 4—SEM backscatter images of H24 temper, (a) Sheet III and (b) Sheet 3. The RD is horizontal and the thickness direction is vertical.

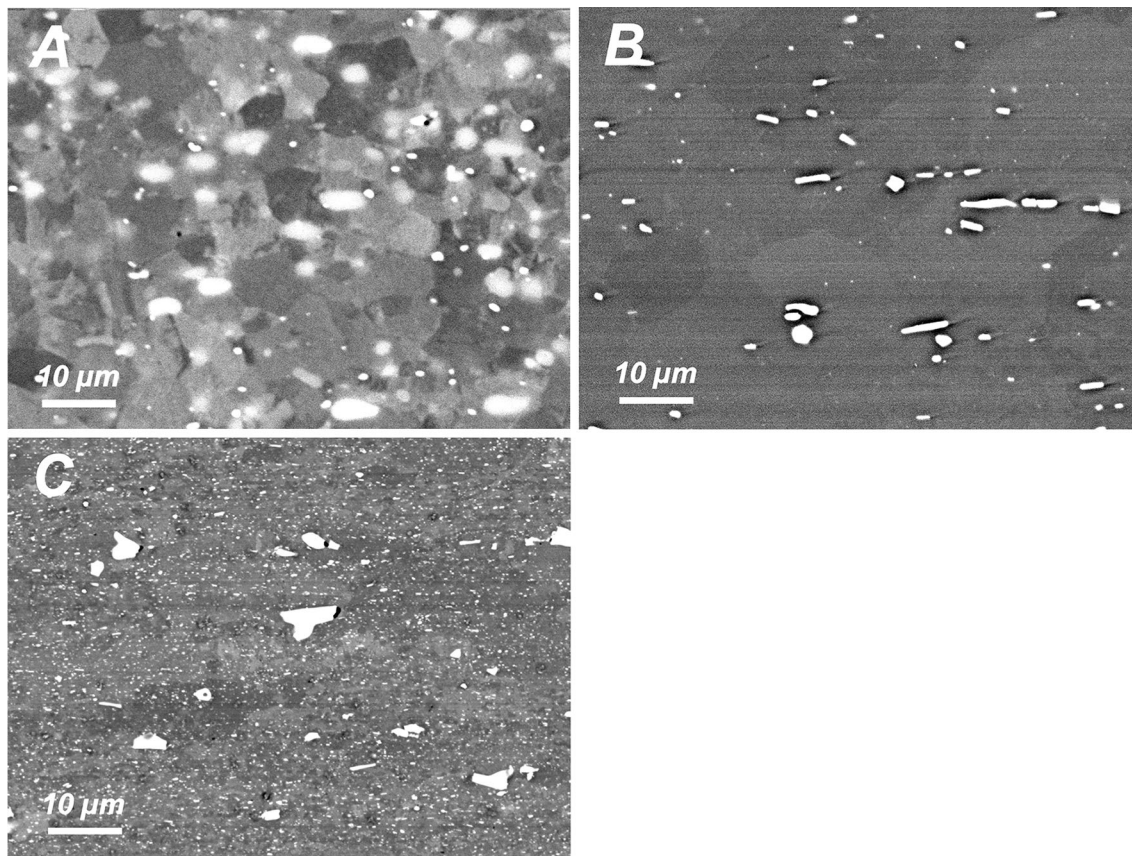


Fig. 5—SEM backscatter images of Sheet III in H24 temper, (a) clad, (b) barrier, and (c) core. The RD is horizontal and the thickness direction is vertical.

and more equi-axed with increasing Mg level. The mean grain size is 50, 35, and 30 μm in the RD and 15, 15, and 13 μm in the thickness direction for Sheets I, II, and III, respectively. No evidence of significant liquid Al-Si penetrating from the clad to the barrier could be found. Since the coarse-grained AA1100 barrier is extremely soft, the TEM specimens made by FIB were damaged by gallium beam, but the Mg_2Si precipitates are still recognizable, *e.g.*, see Figure 7.

The Mg, Si, Mn, and Cu levels measured by SEM-EDX line scanning in Sheets I, II, and III after brazing cycle are shown in Figures 8(a) through (f). To reveal the change from clad through barrier to core more clearly, the averaged and simplified data are re-plotted in Figures 8(g) through (i). The tendency that Si diffuses from clad toward sheet center as well as Mg diffuses from core toward sheet surface is obvious. This leads to the increase of both Si and Mg in the barrier

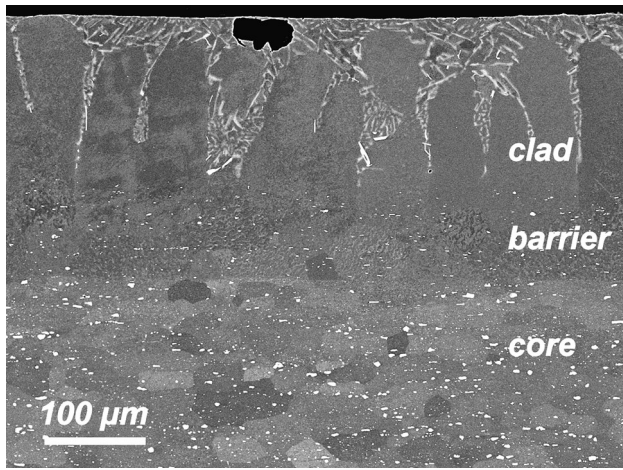


Fig. 6—SEM backscatter image of Sheet III within 1 week after brazing cycle. The RD is horizontal and the thickness direction is vertical.

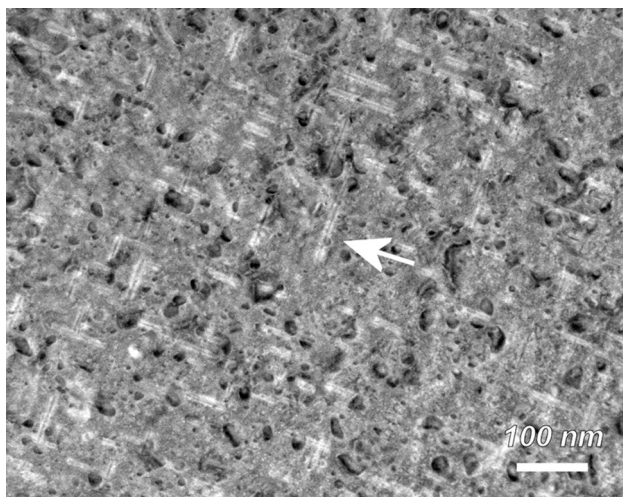


Fig. 7—TEM dark field image showing the Mg_2Si precipitates in the barrier layer of Sheet II in T6 temper. The Mg_2Si precipitates are white and needle-like, with length of ~ 100 nm or less (the arrowed one for example). The black dots are artificially generated by gallium beam during sample preparation.

layer. However, no evidence indicating that Si has diffused into the core or Mg into the clad could be found. The Mn and Cu in the core tend to diffuse toward the sheet surface, the same as Mg. It should be mentioned that the chemistry determined by SEM-EDX is very rough. The contributions from very coarse Si and $Al_6(Mn,Fe)$ particles are not included unless the particles are hit directly by electron beam. Generally speaking, SEM-EDX counts only the elements in solid solution and fine dispersoids, so it often gives lower values.

The microstructure after brazing in Sheets control, 1, 2, and 3 without barrier layer is highly dependent on the Mg level in the core. For Sheet control, which has very low Mg, it has a typical as-brazed microstructure of commercial long-life brazing sheets, with a clear band of dense precipitates (BDP) of 30 to 50 μm in thickness (Figure 9). The clad is of the as-cast dendritic structure

with primary aluminum and Al-Si eutectic, similar to that in Sheets I, II, and III. The core is fully recrystallized with a pancake-like coarse grain structure of ~ 100 μm in grain length and ~ 20 μm in grain thickness (not shown).

As shown in Figure 10, for Sheets 1, 2, and 3 where the Mg content in core is much higher, the as-brazed microstructure is very different from Sheet control. The clad has no typical as-cast dendritic structure; instead, the grains are equiaxed with a number of coarse secondary phase particles in the grain boundary network (Figure 10(a)). The secondary phases include $Al_6(Mn,Fe)$, $\alpha-Al_{15}(Mn,Fe)_3Si_2$, Mg_2Si , and primary Si, as identified by SEM and TEM analyses. Two unique microstructural features were observed: the migration of clad-core interface toward the core side, and the development of GBP-affected zone in the core. The migration distance of clad-core interface increases with the increasing Mg level in core alloy, around 20, 30, and 45 μm for Sheets 1, 2, and 3, respectively. Meanwhile, the depth of GBP increases drastically, from ~ 30 μm in Sheet 1 through ~ 60 μm in Sheet 2 up to ~ 280 μm in Sheet 3.

The microstructure in GBP-affected zone is somewhat similar to the as-cast structure (Figures 10(a) and (b)). The grain structure is equiaxed with ~ 35 μm mean size regardless of the Mg level, and a number of intermetallic particles, mostly $\alpha-Al_{15}(Mn,Fe)_3Si_2$ and Mg_2Si , were observed in both grain boundary and grain interior. The particles in grain boundary are coarse, from several to several ten micrometers, while the ones in grain interior are smaller. Figure 11 shows the $\alpha-Al_{15}(Mn,Fe)_3Si_2$ and Mg_2Si particles in grain interior. The $\alpha-Al_{15}(Mn,Fe)_3Si_2$ is blocky and the Mg_2Si is needle-shaped, both below 1 μm . The fully recrystallized microstructure in the unaffected region of the core is identical to that in Sheets I, II, and III (Figure 10(c)).

Figure 12 shows the change of Mg, Si, Mn and Cu levels across the clad-core interface in Sheet control. The diffusion length is ~ 80 μm for Si, Cu and Mg, but nearly zero for Mn. The Mg, Si, Mn, and Cu levels from clad to core in Sheets 1 to 3 are shown in Figure 13. Since not only solid diffusion but also GBP-induced liquid transportation is involved, the redistribution of alloying elements in Sheets 1, 2, and 3 happens in much wider ranges. The Si has deeply penetrated into the core, about 80, 120, and 380 μm for Sheets 1, 2, and 3, respectively. The thickness of Mg and Cu-depleted zone in the core side is roughly of the same depth. In Sheets 1 and 3, the depleted zone of Mn is similar to that of Mg and Cu, but in Sheet 2, there is no Mn-depleted zone, the same as that in Sheet control. The variation regarding the diffusion of Mn might be due to the uncertainty of EDX measurement.

C. Tensile Properties

Figure 14 shows the tensile strength of Sheet control after brazing cycle from room temperature to 618.15 K (345 $^{\circ}C$). The YS and UTS are nearly constant up to 473.15 K and 373.15 K (200 $^{\circ}C$ and 100 $^{\circ}C$), respectively, but they decrease quickly afterwards, especially

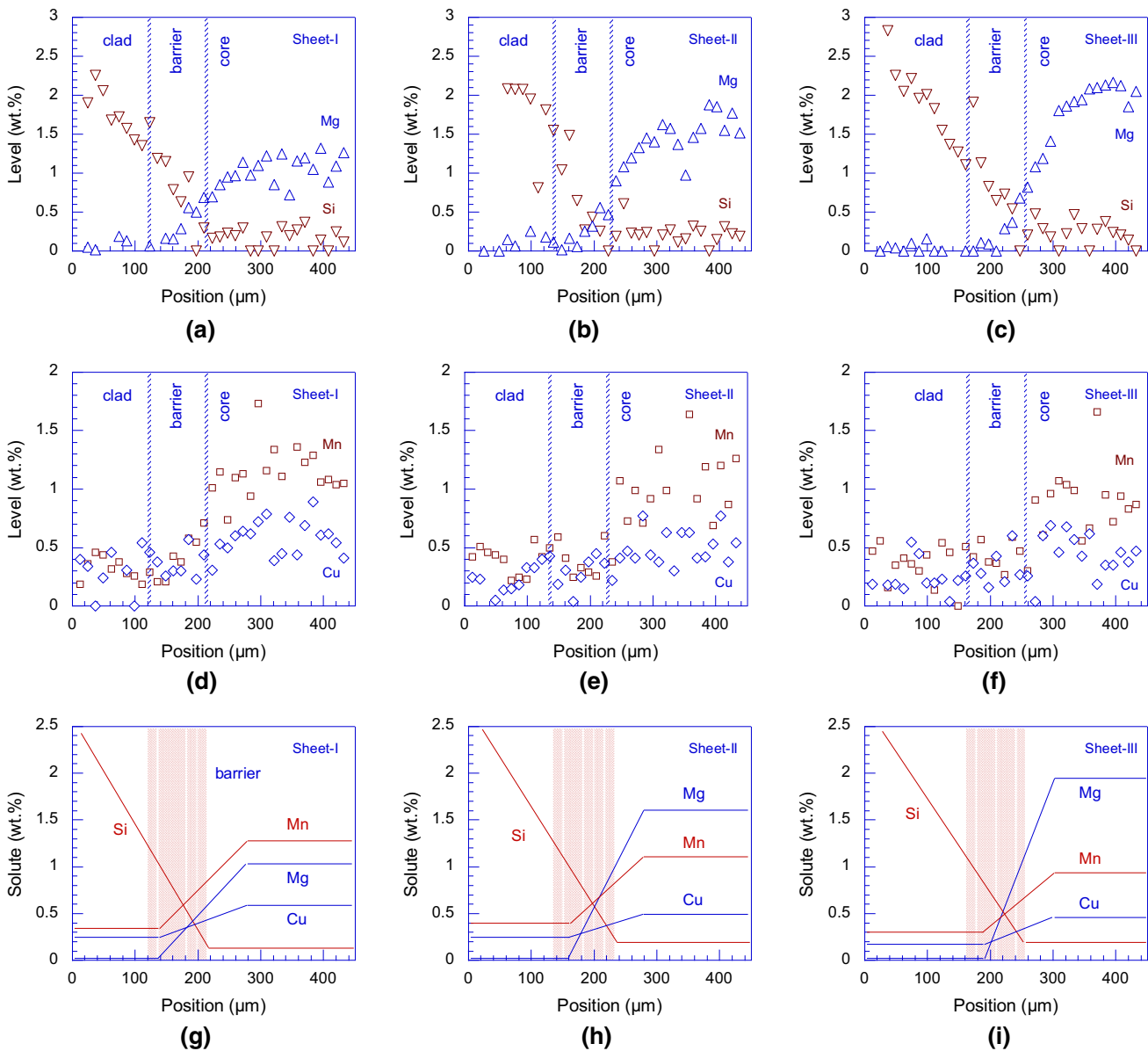


Fig. 8—The levels of alloying elements from clad to core in Sheets I, II, and III within 1 week after brazing cycle, (a) through (c) Mg and Si, (d) through (f) Mn and Cu, and (g) through (i) simplified composition profiles. The origin of x-axis may not be the sheet surface.

the UTS. The room temperature tensile properties of Sheets I, II, and III in W, T4, and T6 tempers are shown in Figure 15 as a function of the Mg level in the core. The YS is very dependent on the temper and it increases significantly from W, T4 to T6, indicating the existence of a strong aging effect. The YS also increases with the increasing Mg, due to the solid solution and grain refinement hardening. The UTS shows the similar tendency, but the T4 and T6 values are not much different, especially when the Mg is low. The fracture EL does not change much from W to T4 temper, but it decreases slightly with the increasing Mg in T6 temper. Figure 16 shows the tensile properties at room temperature of Sheets 1, 2, and 3 without barrier layer. The YS values are very similar to the ones of Sheets I, II, and III, all revealing a strong age hardening effect. However, the

UTS and fracture EL, especially the fracture EL, show a general decreasing tendency with the increasing Mg level in the core.

The YS and UTS of Sheets I, II, and III and Sheets 1, 2, and 3 in T4 temper as a function of temperature are shown in Figures 17 and 18, respectively, and those in T6 temper, in Figures 19 and 20. Approximately, the T4 temper represents the condition of a newly installed heat exchanger, and the high-temperature tensile testing gives its properties when serviced at the testing temperatures. Meanwhile, the T6 temper represents the condition of a heat exchanger being used for a while and reached its maximum age hardening. However, artificial aging occurs unavoidably in the heating-up stage of tensile testing, so the measured properties are not of the true T4 or T6, but more or less over-aged. The YS and UTS of

all the sheets, no matter T4 or T6, show the same trend as Sheet control against temperature. However, in the relatively low temperature range, the sheets with barrier layer have slightly lower YS but somewhat higher UTS than the ones without barrier.

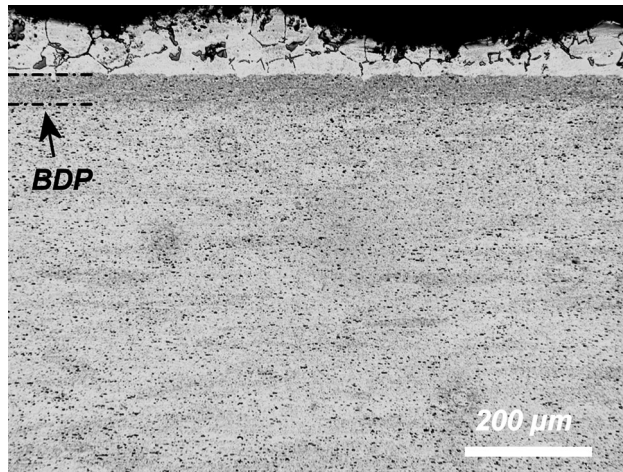


Fig. 9—Optical image of Sheet control after brazing cycle. The RD is horizontal and the thickness direction is vertical.

IV. DISCUSSION

A. Technical Requirements for Core Alloy

When aluminum brazing sheets started to replace copper-based sheets for automotive heat exchangers in early 1970s, the core alloy was initially AA3003 Al-1 pctMn-0.3 pctCu. It was modified to the so-called long-life brazing sheet core alloy in late 1980s and early 1990s, by maximizing the Mn and Cu to 1.2 to 1.5 and 0.5 to 0.7 pct, respectively.^[17,18] Meanwhile, the conventional ingot homogenization at ~ 873.15 K (600 °C) was replaced by re-heating at ~ 793.15 K (520 °C). These modifications lead to the maximized super-saturated Mn and Cu in solid solution and subsequently the maximized solid solution hardening. The impurity Si has been tightly controlled under ~ 0.2 pct, such that when the Si diffuses from the Si-rich clad to the Si-lack core during brazing, the BDP of $\alpha\text{-Al}_{15}(\text{Mn,Fe})_3\text{Si}_2$ forms by phase transformation between Si and solute Mn and/or between Si and $\text{Al}_6(\text{Mn,Fe})$.^[19,20] The BDP acts as a sacrificial layer to protect the rest of core, so corrosion resistance is improved and the long-life is achieved.^[19-21] In most long-life products, the Mg in both the clad and core is tightly controlled under ~ 0.1 pct, in order to keep high braze-ability for Alcan NOCOLOK™ flux brazing process. During the flux brazing, the Mg diffuses to the sheet surface, forming un-dissolvable magnesium

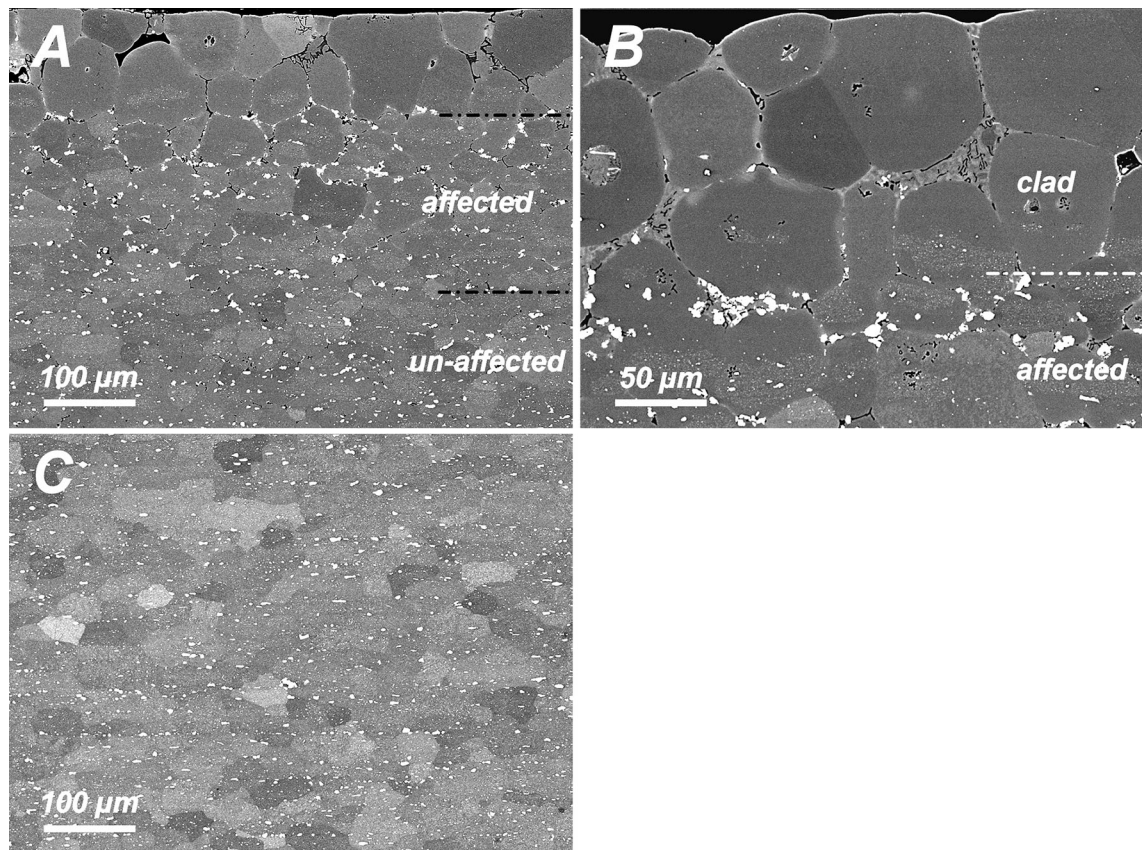


Fig. 10—SEM backscatter images of Sheet 3 within 1 week after brazing cycle, (a) the clad, GBP-affected zone, and unaffected core in low magnification, (b) the clad and GBP-affected zone in high magnification, and (c) the unaffected core. The RD is horizontal and the thickness direction is vertical.

oxides and reacting with the flux to make very coarse detrimental inclusions.^[5,22]

To develop a new aluminum brazing sheet product, especially for high-temperature service, the post-braze YS should be increased in a wide temperature range with no reduction of corrosion resistance or braze-ability. For the AA3xxx core alloys, it is hard to further improve the strength without significant change of chemistry. This is due to the fact that the solid solution hardening from Mn and Cu has already reached the upper limit, which is determined by the cast-ability and solid solubility. The manufacture of core alloys starts from DC casting, which can accommodate up to ~ 1.9 pct Mn. Higher Mn leads to the formation of very coarse $Al_6(Mn,Fe)$ constituents, causing ingot cracking, rolling difficulty, and drastic reduction of sheet formability.^[23,24] Moreover, higher Mn in composition would not increase the Mn in solid solution. This is because the solid solubility of Mn is ~ 0.1 pct at room temperature, and it could not exceed ~ 0.7 pct unless by

specific casting technologies with much higher cooling rate.^[14,25] Although DC casting accommodates quite high Cu, the solubility of Cu at room temperature is ~ 0.3 pct and hard to exceed 0.5 to 0.7 pct.^[14,25] Higher Cu results in the formation of Al_2Cu phase, which reduces the formability and corrosion resistance.^[25] Again, unless much higher cooling rate is enabled during ingot casting, it is difficult to further increase the Cu in solid solution. Considering the productivity and costs, the casting technologies other than DC casting are not favorable.

Besides the intrinsic friction strength, there are dislocation, solid solution, grain boundary, dispersion, and precipitation hardening in aluminum.^[26,27] For most aluminum alloys after exposure at ~ 873.15 K (600 °C), the grain structure is coarse and fully recrystallized so the dislocation and grain boundary hardening effects are negligible. The dispersion hardening in aluminum alloys is usually very limited, unless the volume fraction of particles is very high, *e.g.*, in aluminum matrix composites.^[28] The precipitation hardening could be strong in AA2xxx Al-Cu, AA6xxx Al-Si-Mg, and AA7xxx Al-Zn-Mg-(Cu) alloys. However, the aging temperatures fall into the service temperature range of automotive heat exchangers.^[27] This means the precipitation hardening is unstable during the service, *i.e.*, over-aging occurs and the hardening effect eventually disappears. In addition, the melting temperatures of the eutectics in AA2xxx and AA7xxx are lower than the melting point of Al-Si clad. Although dilute AA7xxx has been patented as core material, AA2xxx and AA7xxx alloys are difficult to be widely used unless the clad alloy and/or the brazing process are significantly changed.^[29] There are research and development activities of using AA6xxx alloys in brazing sheet products.^[30] Although less extensive than that in AA2xxx and AA7xxx, the concerns of lower melting point and over-age softening still exist. Moreover, the high Mg content in AA6xxx reduces the braze-ability for Alcan NOCOLOK™ process, and the high Si prevents the formation of BDP.

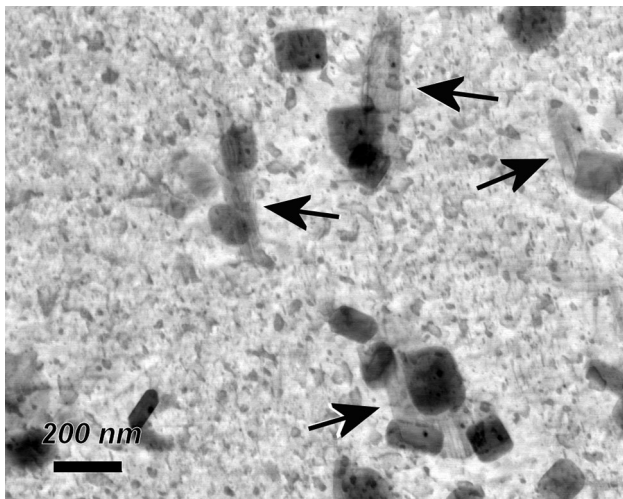


Fig. 11—TEM bright field image showing blocky $\alpha-Al_{15}(Mn,Fe)_3Si_2$ particles and needle-like Mg_2Si particles (the arrowed ones for example) in the GBP-affected zone of Sheet 3 in T6 temper.

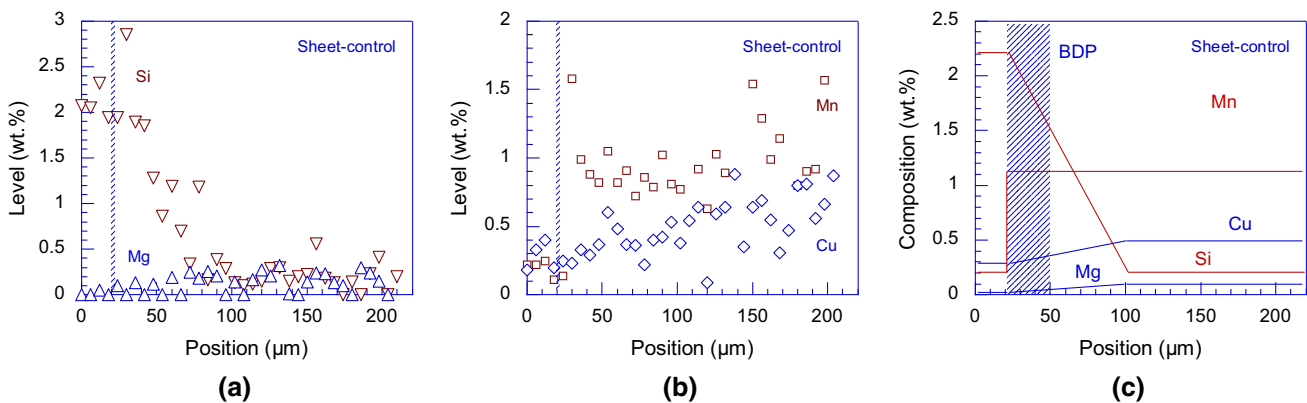


Fig. 12—The levels of alloying elements from clad to core in Sheet control within 1 week after brazing cycle, (a) Mg and Si, (b) Mn and Cu, and (c) simplified composition profiles. The vertical dotted line indicates the location of clad–core interface, but the origin of x-axis is not the sheet surface.

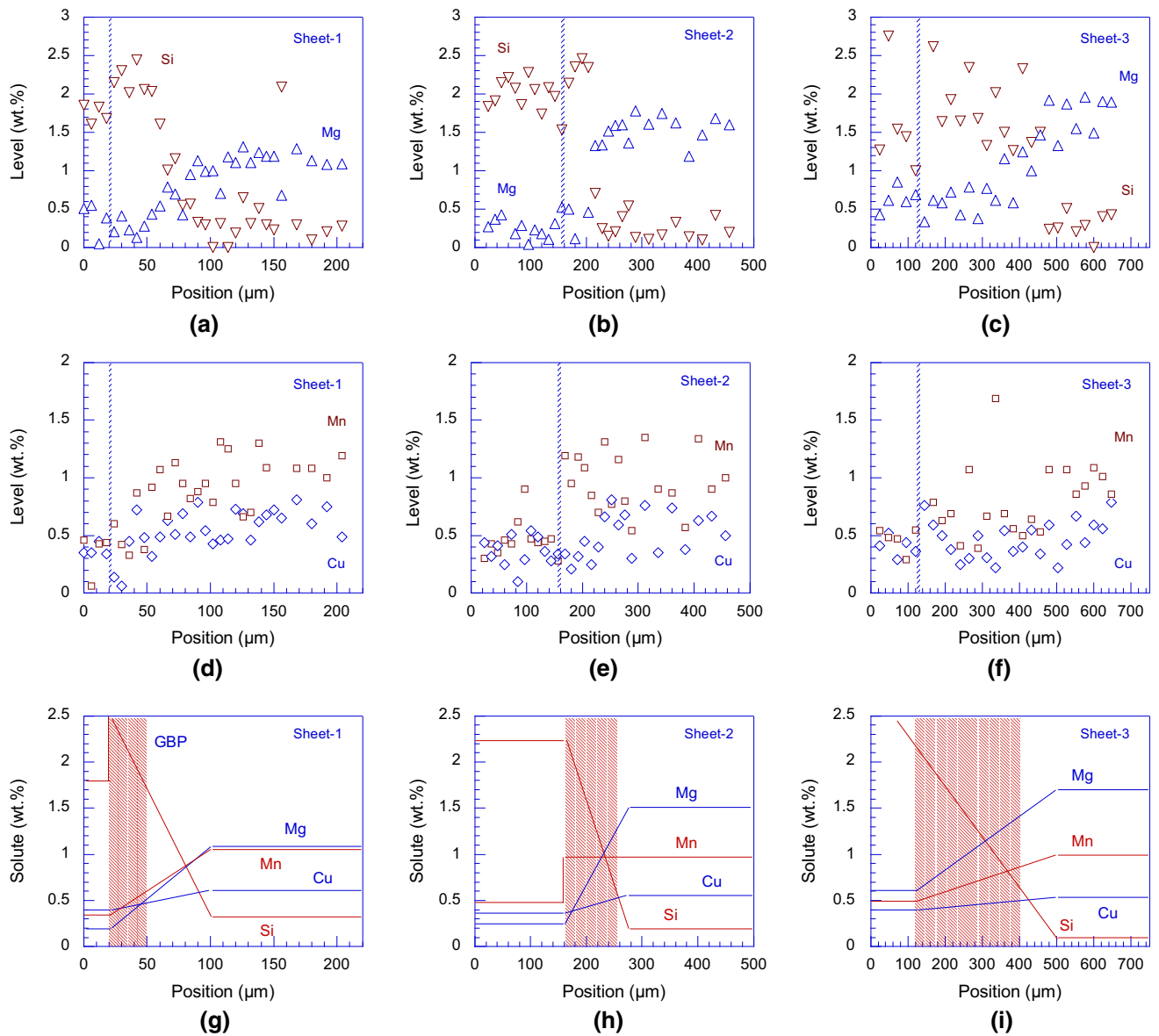


Fig. 13—The levels of alloying elements from clad to core in Sheets 1, 2, and 3 within 1 week after brazing cycle, (a) through (c) Mg and Si (d) through (f) Mn and Cu, and (g) through (i) simplified composition profiles. The vertical dotted line indicates the location of clad-core interface, but the origin of x-axis is not the sheet surface.

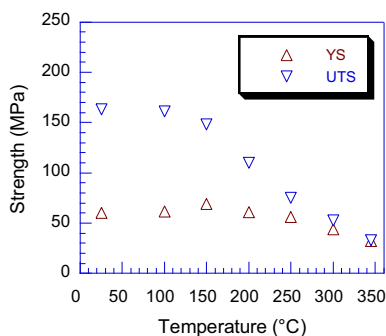


Fig. 14—The YS and UTS of Sheet control as a function of temperature.

It is well accepted that Mg provides strong solid solution hardening, due to its high size misfit and high solid solubility in aluminum.^[26,27,31,32] In a previous work, it was confirmed that this hardening is effective up to 573.15 K (300 °C), which is favorable to the high-performance automotive heat exchangers working at above 473.15 K (200 °C).^[33] The solid solution hardening from Mg is therefore a very efficient strengthening mechanism for the core alloy. The present work shows the negative effects associated with high Mg, *e.g.*, decrease of braze-ability, increase of liquid–solid interaction, and lack of BDP, could be overcome by the introduction of a barrier layer. An increase of strength in a wide temperature range is therefore achievable without reduction of corrosion resistance or braze-ability.

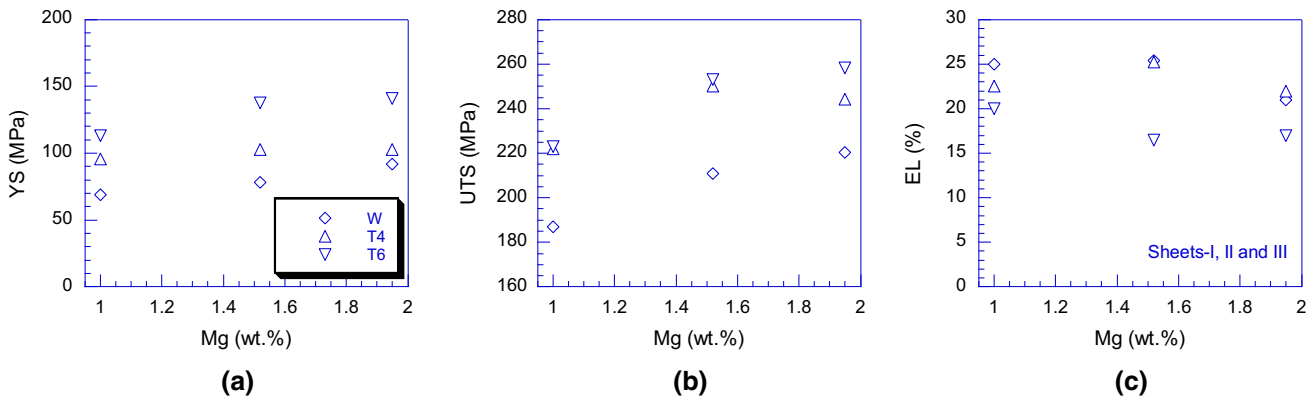


Fig. 15—The room temperature tensile properties of Sheets I to III in W, T4, and T6 tempers as a function of the Mg level in the core, (a) YS, (b) UTS, and (c) fracture EL.

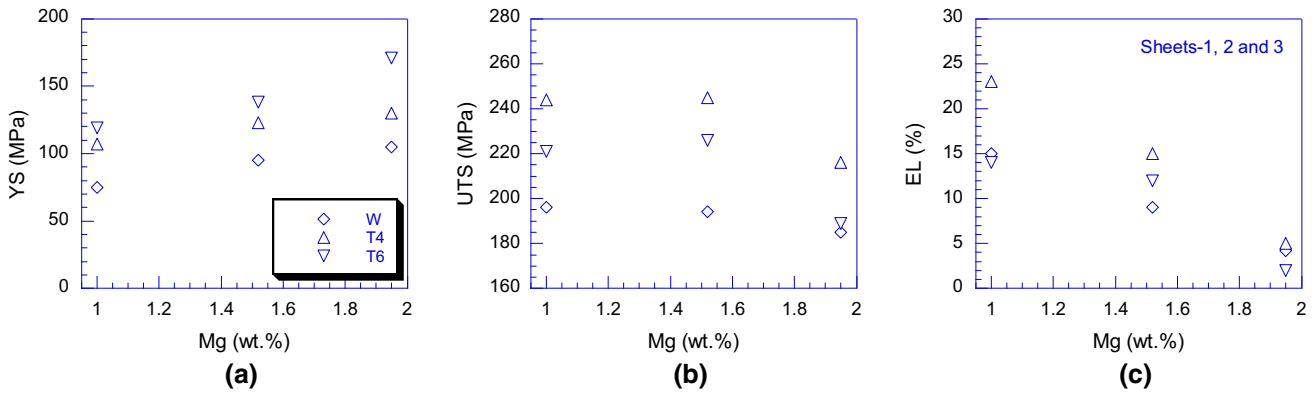


Fig. 16—The room temperature tensile properties of Sheets 1 to 3 in W, T4, and T6 tempers as a function of the Mg level in the core, (a) YS, (b) UTS, and (c) fracture EL.

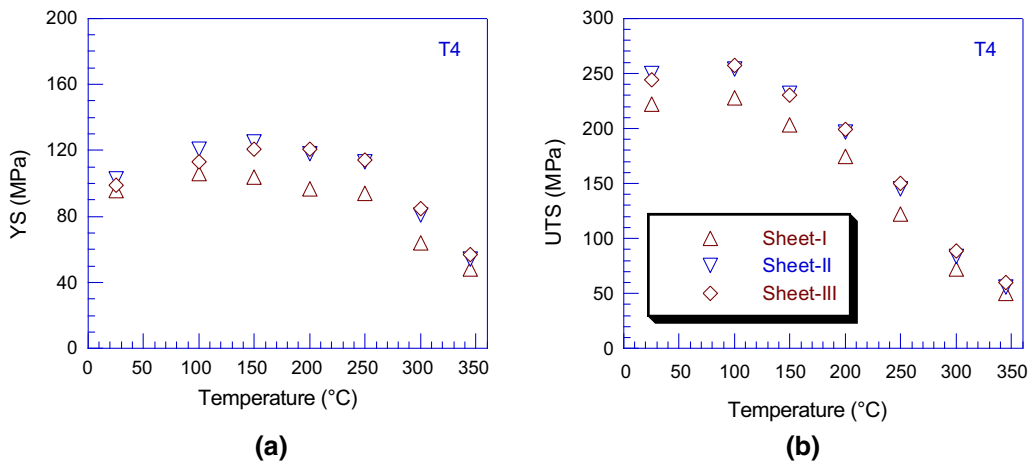


Fig. 17—The tensile properties of Sheets I, II, and III in T4 temper as a function of temperature, (a) YS and (b) UTS.

B. Yield Strength

Theoretically, the tensile properties of layered composites obey the rule-of-mixture, so the post-braze YS of aluminum brazing sheets could be written as

$$\sigma_{\text{sheet}} = f_{\text{clad}}\sigma_{\text{clad}} + f_{\text{barrier}}\sigma_{\text{barrier}} + f_{\text{core}}\sigma_{\text{core}} \quad [1]$$

where σ_{sheet} , σ_{clad} , σ_{barrier} , and σ_{core} are the YS of entire sheet, clad, barrier, and core, respectively, and f_{clad} , f_{barrier} , and f_{core} are the corresponding thickness fractions. The contribution from the clad is negligible, because the re-solidified clad is thin and soft, and during service, it de-bonds from the core due to the corrosion along clad-core interface.^[19–21] Although the AA1100

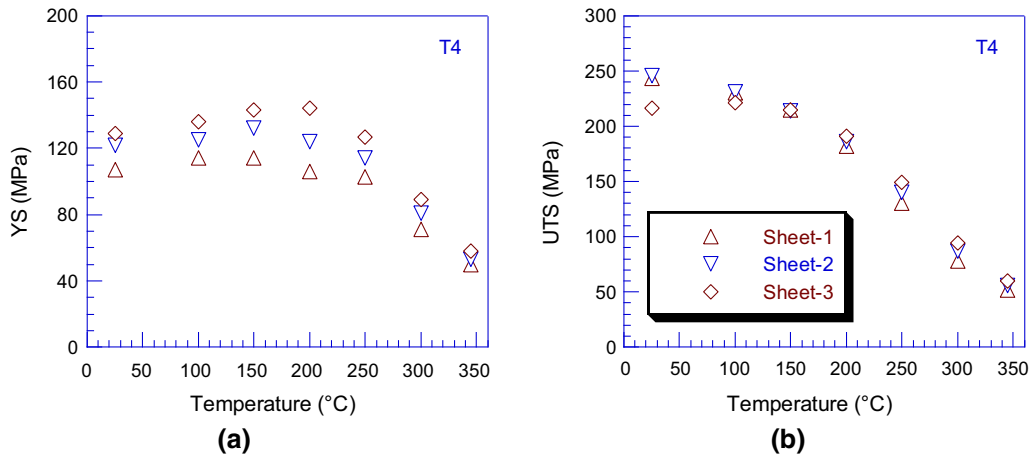


Fig. 18—The tensile properties of Sheets 1, 2, and 3 in T4 temper as a function of temperature, (a) YS and (b) UTS.

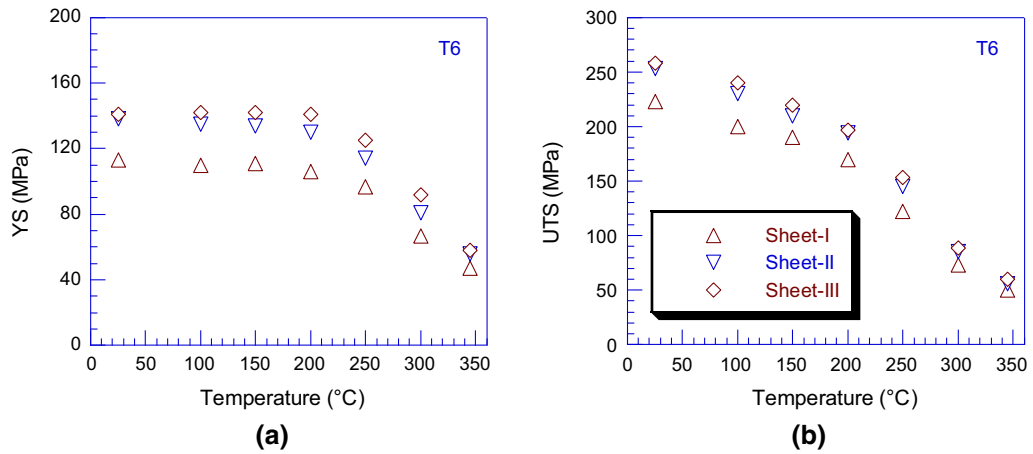


Fig. 19—The tensile properties of Sheets I, II, and III in T6 temper as a function of temperature, (a) YS and (b) UTS.

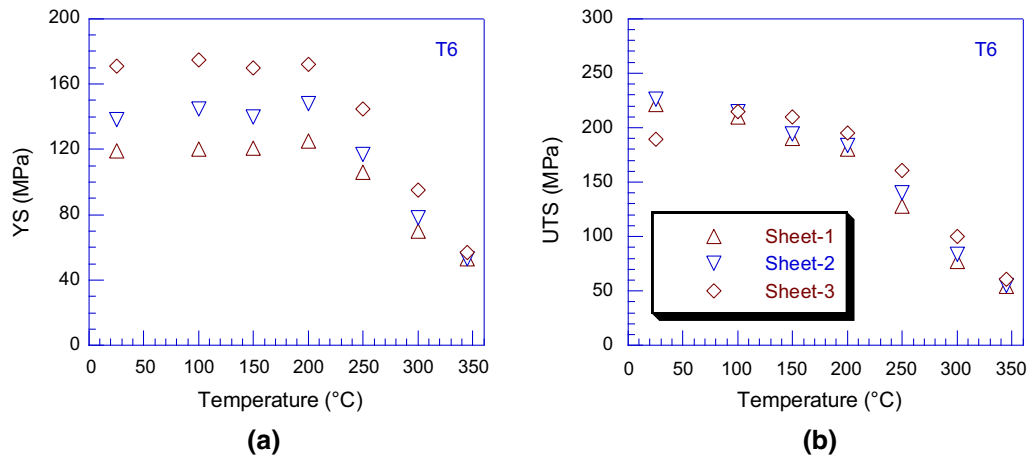


Fig. 20—The tensile properties of Sheets 1, 2, and 3 in T6 temper as a function of temperature, (a) YS and (b) UTS.

barrier alloy is very soft, a significant change of the chemistry occurs during brazing by the inter-diffusion of Si and Mg from clad and core. As shown in Figure 8, after brazing the overall chemistry of the barrier has been changed from 99 pct pure aluminum to a

heat-treatable Al-Si-Mg alloy close to AA6016 Al-0.4 pctMg-1 pctSi. This makes σ_{barrier} vary during service at elevated temperatures. For AA6016 and similar alloys, below 120 °C, the aging response is so slow that it takes several thousand hours to reach the

peak strength, but at higher temperatures, it needs only a few minutes to a few hours.^[34] After reaching the peak strength, further exposure at elevated temperatures leads to over-aging and the YS starts to decrease.

The contribution from the core is simple if no serious liquid–solid interaction, e.g., GBP, occurs. For the Al-Mn-Cu-Mg core alloys, the strength comes from the friction stress of pure aluminum, dispersion hardening from Al₆(Mn,Fe), grain boundary hardening, and solid solution hardening from Mn, Cu, and Mg. When the Mn and Cu contents are constant, the grain boundary hardening and the solid solution hardening from Mg are the only variables. In Reference 33, semi-empirical expressions of σ_{core} have been derived for Al-1.5 pctMn-0.5 pctCu with different Mg levels and grain sizes:

$$\sigma_{\text{core}} = 48.5 + 2.4 \times 10^3 c_{\text{Mg}} + (70 + 3.8 \times 10^3 c_{\text{Mg}}) d^{-\frac{1}{2}} \quad [2]$$

for room temperature to ~ 200 °C, and

$$\sigma_{\text{core}} = (100 - 0.11T) + 0.09Gc_{\text{Mg}} + \left\{ (190 - 0.275T) + \left(-1.59 \times 10^4 + \frac{8.71 \times 10^6}{T} \right) c_{\text{Mg}} \right\} d^{-\frac{1}{2}} \quad [3]$$

for ~ 200 °C to 345 °C, where c_{Mg} is the atomic fraction of Mg in solid solution, d is the mean grain size, G is the shear modulus, and T is the absolute temperature. These equations were derived assuming DC casting and ingot re-heating at ~ 793.15 K (520 °C). For other casting techniques and/or conventional ingot homogenization at ~ 873.15 K (600 °C), the terms related to solid solution hardening from Mn and Cu should be modified.

In Figure 21, the theoretical YS values of A, B, and C core alloys calculated by Eqs. [2] and [3] are plotted against temperature. Comparing Figures 17 through 20 with Figure 21, the YS values of newly developed brazing sheets, with or without barrier layer, follow the same trend of their core alloys in both T4 and T6 tempers. Each sheet is stronger than its core alloy in the temperature range from room temperature to ~ 523.15 K (250 °C), especially in T6 temper, confirming the existence of precipitation hardening in the

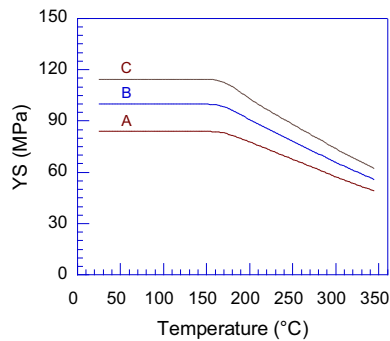


Fig. 21—The calculated YS of Alloys-A, B and C as a function of temperature.

barrier layer and GBP-affected zone. When the temperature approaches ~ 573.15 K (300 °C), the strength of entire sheet starts to decrease faster than its core alloy. This is likely because the over-aging effect in the heating-up stage of tensile testing becomes strong. As shown in Figures 15 and 16, the room temperature UTS and EL of Sheets 1 to 3 without barrier layer have a decreasing tendency with the increasing Mg content. Meanwhile, Sheets I to III with barrier layer show an increasing tendency of UTS with the increasing Mg, and the EL decreases only slightly. This indicates that the barrier layer helps to maintain the high work hardening and ductility of the high Mg core.

C. Corrosion Resistance and Braze-Ability

The barrier layer is also critical for the corrosion resistance and braze-ability. The corrosion resistance of aluminum is very dependent on alloying elements and microstructure. In the present work, two types of corrosion might be involved: uniform corrosion and secondary phase induced local galvanic corrosion. The atoms of an alloying element within solubility stay in solid solution, while excess atoms form secondary phase particles. For commercial pure aluminum-like AA1100, the corrosion potential against saturated calomel electrode, E_{SCE} , is about -750 mV, but it may change when solid solution atoms are present.^[35,36] For example, as shown in Figure 22, the corrosion potential is increased by Mn, Cu, and Si, but reduced by Mg.^[36] An increase of the potential indicates higher corrosion resistance. In general, the contributions from different elements can be summed, and the resultant overall potential controls the rate of uniform corrosion.

When the alloying elements form secondary phase particles, local galvanic corrosion occurs if the potential of secondary phase is very different from that of aluminum matrix. For the present work, the major secondary phases include Si, $\alpha\text{-Al}_{15}(\text{Mn,Fe})_3\text{Si}_2$, Mg_2Si , and $\text{Al}_6(\text{Mn,Fe})$. The potentials of Si and $\alpha\text{-Al}_{15}(\text{Mn,Fe})_3\text{Si}_2$ are ~ 490 and ~ 300 mV higher than pure aluminum, respectively, and that of Mg_2Si is ~ 840 mV lower than pure aluminum.^[37–39] This leads to intensive galvanic reaction around the Si, $\alpha\text{-Al}_{15}(\text{Mn,Fe})_3\text{Si}_2$ and Mg_2Si particles and consequently the preferential attack of the region with high population

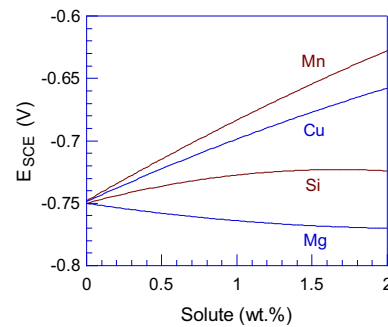


Fig. 22—Effects of Mn, Cu, Si, and Mg in solid solution on the corrosion potential of AA1100 pure aluminum, derived from Ref. [36].

density of these particles. The corrosion potential of $\text{Al}_6(\text{Mn,Fe})$ is only slightly more cathodic than pure aluminum, so it is considered harmless.^[38] Both the rate and direction of corrosion are critical to prevent rapid through-thickness attack. In commercial long-life Al-Si/Al-Mn-Cu brazing sheets, this is achieved by manipulating the uniform corrosion, *i.e.*, solid solution levels of Mn, Cu, and Si, and the local galvanic corrosion, *i.e.*, population density and spatial distribution of $\alpha\text{-Al}_{15}(\text{Mn,Fe})_3\text{Si}_2$ particles.^[19–21]

When the solute levels of Mn, Cu, Si, and Mg are known, the overall potential of aluminum matrix could be calculated according to Figure 22. The Mn, Cu, Si, and Mg contents in Sheet control are given by Figure 12, but they consist of contributions from both solid solution and small secondary phase dispersoids. Based on binary phase diagrams and a comprehensive study of Al-Si/Al-Mn-Cu brazing sheets with electron probe micro-analyzer (EPMA), the maximum super-saturated solute level of Si in the clad is ~ 1.2 pct and that of Mn in the core is ~ 0.7 pct.^[14,25] Meanwhile, the 0.5 pct Cu and 1 to 2 pct Mg are believed all in solid solution, since Cu and Mg have high solubility limits. Using this information, Figure 12 can be adjusted to approximately represent merely the Mn, Cu, Si, and Mg in solid solution (Figure 23(a)). Using Figures 22 and 23(a), the effect of each solute element on the potential is calculated, and the results including their sum are plotted in Figure 23(b). The overall corrosion potential increases monotonically from -693 mV in the clad through a diffusion distance of ~ 80 μm , including the BDP, to -670 mV in the core.

Nevertheless, there is local galvanic reactions in the clad and BDP, due to Al-Si eutectics and high population density of $\alpha\text{-Al}_{15}(\text{Mn,Fe})_3\text{Si}_2$ particles, respectively. As shown in Figure 9, the eutectics in the clad are coarse and heterogeneously distributed, so the galvanic reaction in the eutectics is unable to be integrated into uniform corrosion. On the contrary, the $\alpha\text{-Al}_{15}(\text{Mn,Fe})_3\text{Si}_2$ particles in the BDP are fine and evenly distributed, so the local galvanic reaction can be integrated into uniform corrosion, resulting in an apparent corrosion potential of ~ 30 mV lower than the core.^[19–21] When this effect is considered, a modified

profile is obtained in Figure 23(c). It should be mentioned that the potential of -693 mV of the clad represents the coarse α -aluminum grains only, because the potentials of Si and aluminum are so different that the Al-Si eutectics dissolve very quickly.^[39] Figure 23(c) is consistent with the general observation in commercial long-life brazing sheets that the corrosion in BDP is faster than the residual clad, and that in residual clad is faster than the core.^[19–21] This means when corrosive attack breaks through the eutectics in the clad and reaches the BDP, it changes the direction from through-thickness to lateral, so it would not go into the rest of core until a large portion of BDP is consumed.

Similarly, in Figure 24, the profiles of solutes and corrosion potentials in Sheets 1, 2, and 3 are plotted. The higher Mg in the core yields two critical differences from Sheet control: (i) the corrosion potential of the core is more negative than the clad, and (ii) the solid diffusion-controlled BDP is replaced by the liquid transportation controlled GBP. As shown in Figure 11, there exists a high population density of $\alpha\text{-Al}_{15}(\text{Mn,Fe})_3\text{Si}_2$ and Mg_2Si particles in the GBP-affected zone. Since the corrosion potential of Mg_2Si particles is only -1596 mV, they dissolve very quickly and release Mg into solid solution.^[38] This reduces the corrosion potential of aluminum matrix and promotes the local galvanic reaction between $\alpha\text{-Al}_{15}(\text{Mn,Fe})_3\text{Si}_2$ and aluminum. Hence, with regard to sacrificial effect, the GBP-affected zone is equivalent to the BDP. To illustrate this effect, in Figures 24(g) through (i), an offset of -30 mV, the same as that in BDP, is given to the GBP-affected zone. However, intensive intergranular corrosion may occur in the GBP-affected zone, making the dissolution much faster than that in the BDP. The GBP-affected zone could be much deeper and harder to control than the BDP, resulting in significant reduction of the work hardening and ductility, as shown in Figures 16(b) and (c).

The profiles of solute elements and corrosion potentials in Sheets I, II, and III are shown in Figure 25, which appear similar to those of Sheets 1, 2, and 3. However, the AA1100 barrier layer makes for two important differences: (i) there is no detrimental GBP

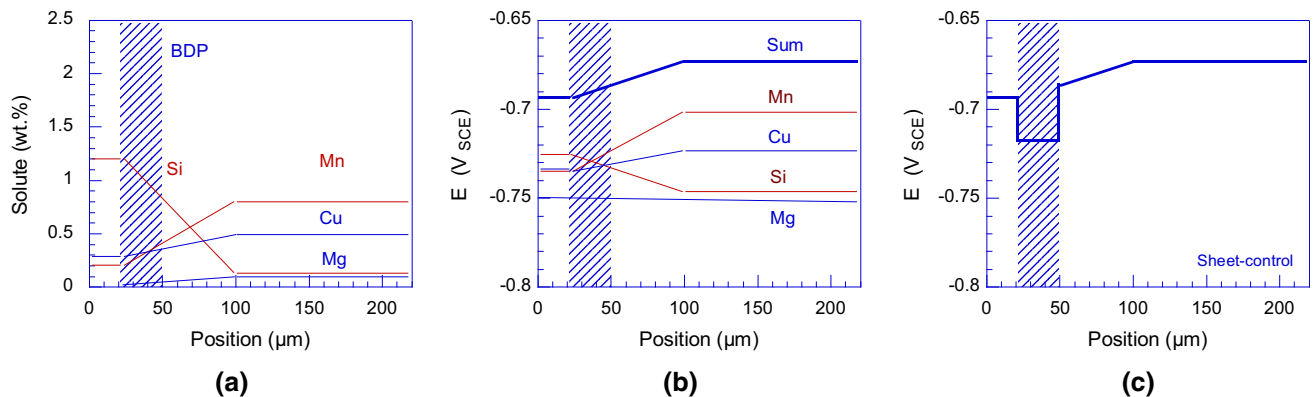


Fig. 23—The profiles of (a) solutes, (b) contribution of solute elements to corrosion potential, and (c) apparent corrosion potential with consideration of BDP for Sheet control.

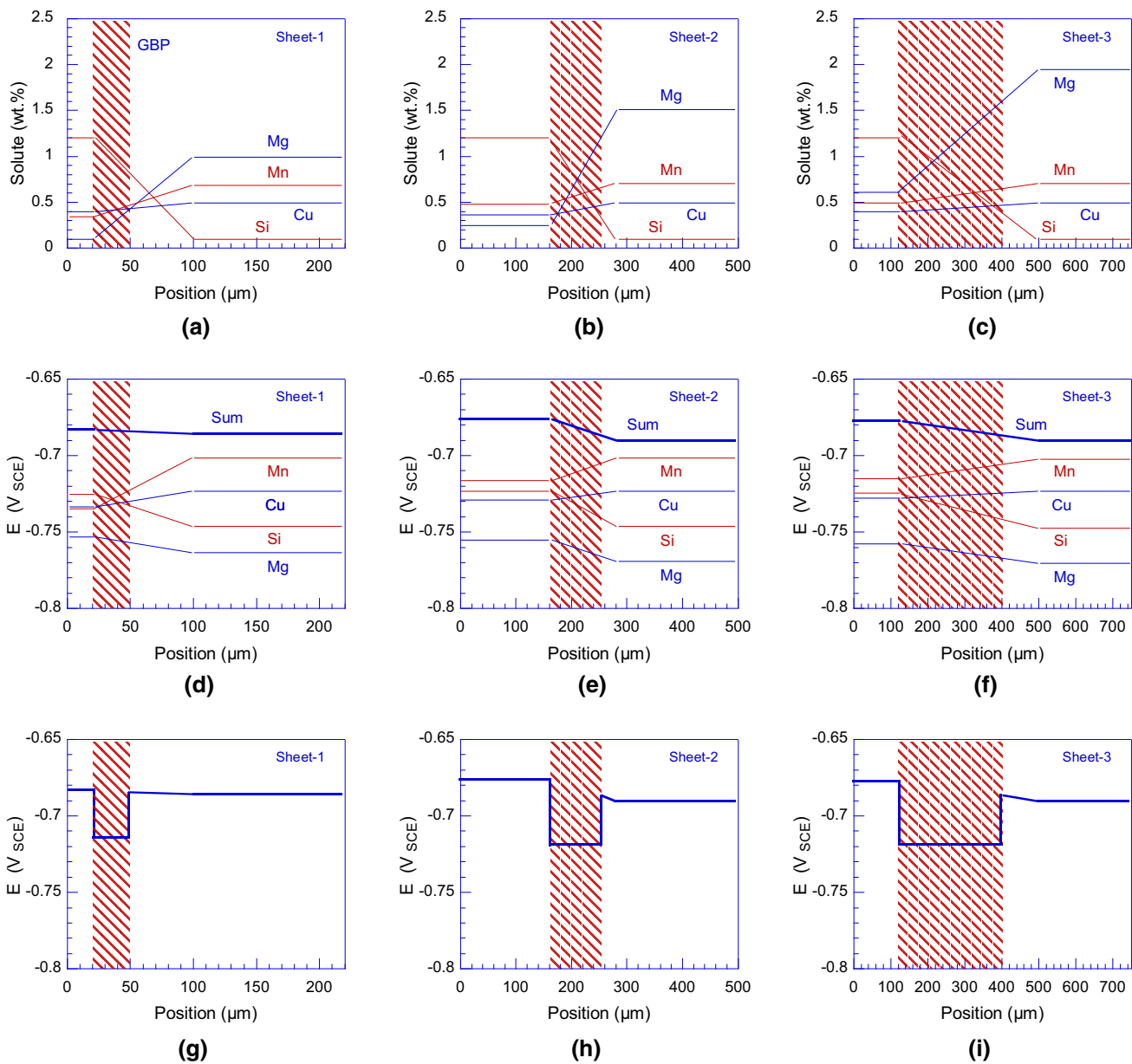


Fig. 24—(a) through (c) the solute profiles of Sheets 1, 2, and 3, respectively, (d) through (f) the corrosion potential profiles based on solute level only, and (g) - (i) the apparent corrosion potential profiles considering both the solute level and the sacrificial effect from the $\alpha\text{-Al}_{15}(\text{Mn,Fe})_3\text{Si}_2$ and Mg_2Si particles in the GBP-affected zone.

and (ii) the sacrificial layer thickness is controllable. Since AA1100 has very high melting point at $\sim 933.15\text{ K}$ ($660\text{ }^\circ\text{C}$), it remains solid through the brazing cycle and acts as a physical isolator to prevent the molten Al-Si from contacting the core. Hence, there is no liquid transportation but only solid diffusion, and the detrimental effects of GBP on corrosion resistance or mechanical properties no longer exist. As the Si diffused from the clad encounters the Mg diffused from the core, a high population density of Mg_2Si particles is generated in the barrier layer, making the layer a sacrificial band (Figure 7). This band is similar to the BDP in Sheet control but different from the GBP-affected zone in Sheets 1, 2, and 3, because no intergranular reaction is involved. Since the barrier layer has very coarse grain

size, the diffusion of alloying elements is controlled by lattice diffusion.

The lattice diffusivity, D , as a function of temperature is given by

$$D = D_0 \exp\left(\frac{-Q}{RT}\right) \quad [4]$$

where D_0 is the pre-exponential factor, Q is the activation energy, and R is the gas constant equal to $8.314\text{ Jmol}^{-1}\text{K}^{-1}$. The diffusion length, λ , for time, t , is given by

$$\lambda = \sqrt{Dt} \quad [5]$$

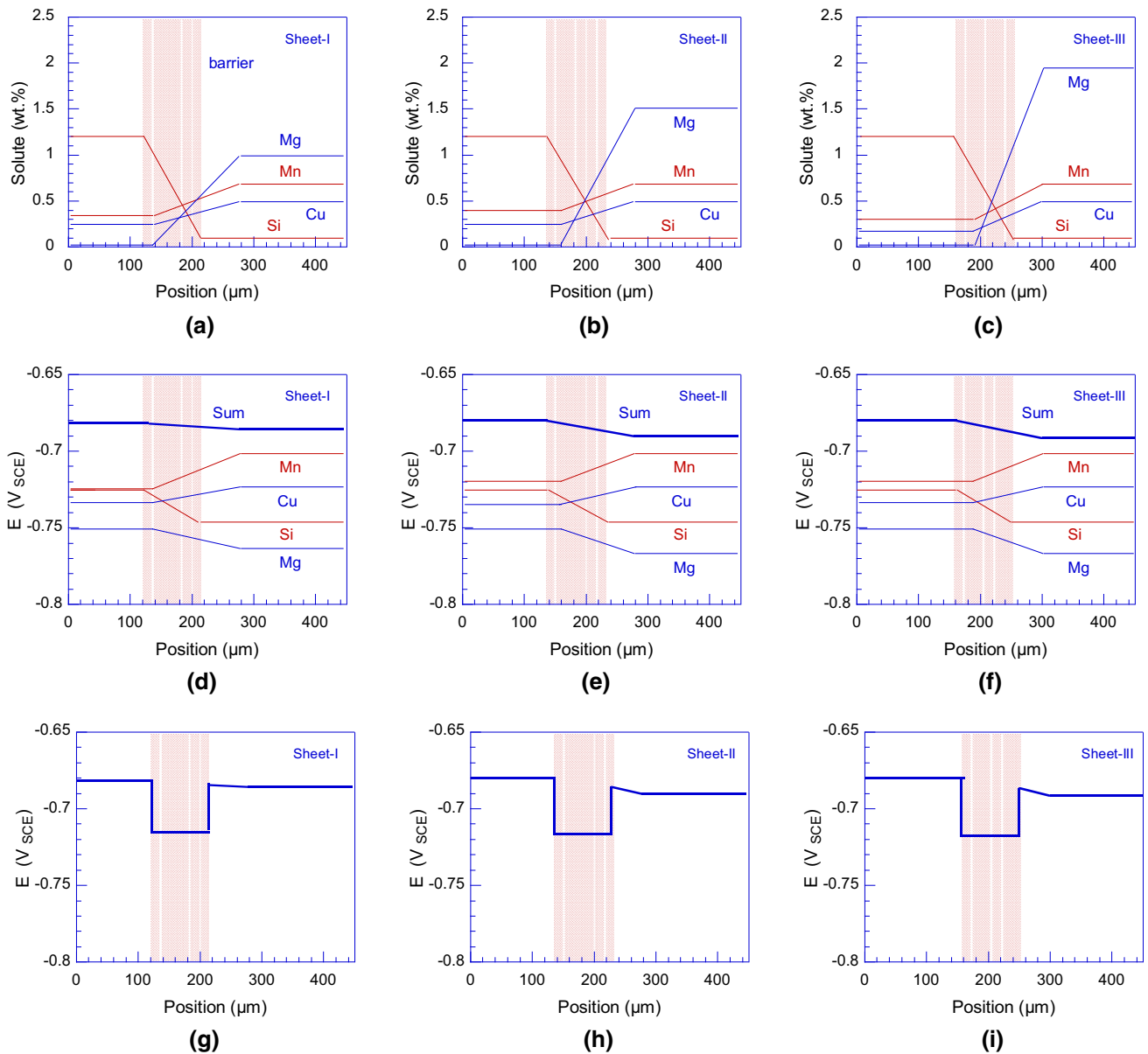


Fig. 25—(a) through (c) the solute profiles of Sheets I, II, and III, respectively, (d) through (f) the corrosion potential profiles based on solute level only, and (g) through (i) the apparent corrosion potential profiles considering both the solute level and the sacrificial effect from the Mg_2Si particles in the barrier layer.

Depending on the methodologies of measurement and calculation, the values of D_0 and Q vary in wide ranges. In Table II, some moderate values of D_0 and Q for Mn, Cu, Si, and Mg from literatures are listed.^[40–43] Using these values, the diffusivities at 873.15 K (600 °C) and the diffusion length for 3 minutes are calculated by Eqs. [4] and [5], respectively. The results, as listed in Table II, indicate the diffusion of Mg, Si, and Cu is much faster than Mn and the diffusion length values are all within 20 μm . When comparing to the chemical composition profiles determined by SEM-EDX (Figure 8), the calculated values of diffusion length appear somewhat shorter. This may be because of (i) the values of D_0 and Q are not accurate enough, (ii) the contribution from grain boundary diffusion is not

included, and (iii) the formation of $\alpha-Al_{15}(Mn,Fe)_3Si_2$ and Mg_2Si may affect the diffusion rates. Nevertheless, the calculation does indicate as long as the barrier layer is thick enough, the Mn, Cu, and Mg in the core have little chance to diffuse across the barrier to the clad, nor does the Si from the clad to the core.

To ensure high braze-ability for commercial flux brazing processes, e.g., Alcan NOCOLOK™ process, it is essential to keep the Mg content in sheet surface very low. Assuming the clad is fully or mostly melted upon brazing, the clad–core interface can be considered equivalent to the sheet surface. For the conventional brazing sheet products, e.g., Sheet control, both clad and core must have very low Mg; otherwise, the molten Al–Si unavoidably contains high concentration of Mg.

Table II. The Pre-exponential Factor D_0 , Activation Energy Q , Diffusivity at 600 °C and Diffusion Length for 3 Min at 600 °C for Mn, Cu, Si, and Mg in Aluminum

T (°C)	Mn	Cu	Si	Mg
D_0 ($\text{m}^2 \text{s}^{-1}$)	8.7×10^{-3}	6.54×10^{-5}	2.02×10^{-4}	6.6×10^{-5}
Q (kJ mol^{-1})	208.0	136.0	136.0	124.5
$D_{600^\circ\text{C}}$ ($\text{m}^2 \text{s}^{-1}$)	2.98×10^{-15}	4.59×10^{-13}	1.43×10^{-12}	2.28×10^{-12}
$\lambda_{600^\circ\text{C } 3\text{min}}$ (m)	7.3×10^{-7}	9.1×10^{-6}	1.6×10^{-5}	2.0×10^{-5}

For example, the surface of clad side in Sheets 1, 2, and 3 turns dark gray after brazing, indicating the extensive surface oxidation of Mg. With a barrier layer thicker than the diffusion length, *e.g.*, $\sim 20 \mu\text{m}$ at 873.15 K (600 °C) for 3 minutes, the Mg in the core cannot reach the clad–barrier interface, so the braze-ability is independent of the chemistry of core alloy. This is confirmed by the fact that the surface of clad side in Sheets I, II and III after brazing cycle remains light gray, the same as Sheet control.

D. Fabrication and Applications

For the newly developed brazing sheet product, the clad can be any commercial Al-Si filler alloys, *e.g.*, AA4343 (Al-7.5 pctSi), AA4045, and AA4047 (Al-12 pctSi). The core would contain 1.0 to 2.0 pct Mg, 1.0 to 1.5 pct Mn, 0.3 to 0.7 pct Cu, < 0.2 pct Si, and < 0.25 pct Fe, other elements each < 0.1 pct and total < 0.3 pct, balance aluminum. The barrier could be made of inexpensive AA1xxx or other dilute alloys, as long as the solidus is high and the recrystallization and grain coarsening are prone. It is well known that the GBP is very dependent on whether the core or barrier could be fully recrystallized before the clad starts to melt during the brazing process.^[14,16,44–46] Since the AA1100 barrier has very low temperature for recrystallization and grain growth regardless of the temper or pre-strain level, *e.g.*, see Reference 47, there is no concern of GBP for the present work. The barrier layer should be thicker than the diffusion length of Mg, namely around $20 \mu\text{m}$, for commercial flux brazing processes. Meanwhile, the soft barrier should not be too thick; otherwise, the reduction of the strength of entire sheet might be a concern. The new brazing sheets could be supplied in cold rolled H1x or partially annealed H2x tempers, the same as most commercial products. Since the detrimental liquid–solid interactions, *e.g.*, GBP, are prevented by the barrier layer, the new sheet product could also be supplied in very formable fully annealed O temper. This will greatly facilitate the fabrication of heat exchangers with complex shape profiles by reducing the spring-back and die wearing.

The fabrication of the new product is similar to that of commercial Al-Si/Al-Mn-Cu long-life sheets, consisting of DC casting, ingot scalping, re-heating, roll-bonding, hot rolling, cold rolling, and batch annealing. The barrier layer can be added by regular hot roll-bonding or by a combination of co-casting and roll-bonding. The regular hot roll-bonding route starts with DC casting of

the clad, barrier, and core ingots, followed by ingot scalping of the shell zone from each rolling face. The clad and barrier ingots are re-heated to $\sim 773.15 \text{ K}$ (500 °C) and hot rolled to the proper hot band gauges, which are determined by the core ingot thickness, the required thickness fractions of clad and barrier, and either single-side or double-side cladding. The hot bands of clad and barrier are welded to the core ingot, re-heated to no more than 793.15 K (520 °C), hot rolled heavily, followed by cold rolling down to the final gauge. The final gauge sheet could go through batch annealing to reach partial or full recrystallization for improved formability. For the route with combination of co-casting and roll-bonding, the barrier and core alloys are cast into one ingot, while the core alloy solidifies first and the barrier alloy is cast on the surface of core alloy. The rest of thermo-mechanical processing is the same.

The worldwide demand for high-performance heat exchangers and dissipaters increases continuously. While aluminum brazing sheets provide a unique advantage in light-weighting over copper alloys and stainless steels, their applications are restricted by the short of strength at elevated temperatures. The present work shows it is possible to raise the peak service temperature of aluminum heat exchangers to $\sim 573.15 \text{ K}$ (300 °C) by modifying the chemistry and laminated structure of brazing sheet, without sacrifice of corrosion resistance or braze-ability. This will facilitate the down-gauging of automotive heat exchangers for weight reduction and promote the use of super/turbo-charged engines with better fuel efficiency and smaller size.

V. CONCLUSION

1. A high-strength aluminum brazing sheet product has been developed for automotive heat exchangers. It consists of regular Al-Si clad, newly designed Al-Mn-Cu-Mg core, and 99 pct pure aluminum barrier between the clad and core. Comparing to the conventional long-life Al-Mn-Cu core alloys, the addition of Mg provides a very strong hardening effect in a wide temperature range. The post-braze strength of the new sheet product is therefore significantly higher than the conventional Al-Si/Al-Mn-Cu products, and the high strength is maintained at elevated temperatures up to $\sim 573.15 \text{ K}$ (300 °C).

- When the Al-Si clad contacts the high Mg core directly, a very extensive liquid–solid reaction, GBP, occurs upon brazing, leading to degrading of ductility and corrosion resistance. The function of barrier layer is to separate the clad and core physically, thus prohibiting the molten Al-Si to penetrate into the core along grain boundaries. The barrier layer also prevents the solid diffusion of Si from the clad into the core, and Mg from the core to the sheet surface. The very low level of Mg in the sheet surface ensures high braze-ability for commercial flux brazing processes.
- After brazing and natural or artificial aging, a high population density of Mg₂Si precipitates is generated in the barrier layer due to the Si and Mg in-diffused from the clad and core, respectively. This makes the apparent corrosion potential of the barrier layer more negative than the core, the same as the BDP in conventional Al-Si/Al-Mn-Cu long-life brazing sheets. The barrier layer is therefore not only a physical separator but also a sacrificial band in corrosive environment. Hence, the corrosion resistance of new brazing sheet product is significantly improved.
- The new brazing sheet product, having high strength, good corrosion resistance, and good braze-ability, is suitable to the high-performance automotive heat exchangers with peak service temperature at 473.15 to 573.15 K (200 to 300 °C). It is also beneficial for heat exchangers used within regular service temperature range below 423.15 K (150 °C), since the high strength enables decrease of sheet thickness, leading to weight reduction and better heat exchange efficiency. The fabrication of the new sheet product is very similar to that of commercial Al-Si/Al-Mn-Cu long-life brazing sheets.

ACKNOWLEDGMENT

This work was supported by Natural Resources Canada through P-002605.001. Dr. B. Shalchi Amirkhiz is appreciated for the TEM analysis.

REFERENCES

- M.M. Schwartz: *Brazing*, ASM International, Materials Park, 1987.
- G. Humpston and D.M. Jacobson: *Principle of Soldering and Brazing*, ASM international, Materials Park, 1991.
- R. Woods: *CAB Brazing Metallurgy, 12th Annual International Invitational Aluminum Brazing Seminar*, AFC Holcroft, Novi, 2007.
- M.P. Groover: *Fundamentals of Modern Manufacturing: Materials Processes and Systems*, Wiley, Hoboken, 2007.
- J. Liu: *NOCOLOK Flux and Aluminum Brazing*, SAE Technical Paper 960244, 1996.
- H. Jin, J. Liang, Y. Zeng, and M.S. Kozdras: *SAE Int. J. Mater. Manf.*, 2015, vol. 8 (3), pp. 736–43.
- H. Jin, M.S. Kozdras, B. Shalchi-Amirkhiz, and S.L. Winkler: *Metall. Mater. Trans.*, 2018, vol. 49A, pp. 3091–3108.
- F.P. Incropera, D.P. DeWitt, T.L. Bergman, and A.S. Lavine: *Introduction to Heat Transfer*, Wiley, Hoboken, 2007.
- E.A.D. Saunders: *Heat Exchanges: Selection, Design and Construction*, Wiley, New York, 1988.
- J.B. Heywood: *Internal Combustion Engine Fundamentals*, McGraw-Hill, New York, 1988.
- B. Hu, J.W.G. Turner, S. Akehurst, C. Brace, and C. Copeland: *J. Auto. Eng.*, 2017, vol. 231 (4), pp. 435–56.
- H. Jin: *Metall. Mater. Trans.*, 2019, vol. 49A, pp. 3091–3108.
- M. Nylén, U. Gustavsson, B. Hutchinson, and A. Örtinä: *Mater. Sci. Forum*, 2000, vols. 331–337, pp. 1737–42.
- S.D. Meijers: *Corrosion of aluminium brazing sheet*, Ph.D. Thesis, Delft University of Technology, 2002.
- A.J. Wittebrood, S. Desikan, R. Boom, and L. Katgerman: *Mater. Sci. Forum*, 2006, vols. 519–521, pp. 1151–56.
- A. Wittebrood: *Microstructural changes in brazing sheet due to solid-liquid interaction*, Ph.D. Thesis, Delft University of Technology, 2009.
- P.E. Fortin, P.H. Marois and D.G.S. Evans: *US Patents 5037707 and 5041343*, August 1991.
- A. Gray, G.J. Marshall and A.J.E. Flemming: *International Patent WO 94/22633*, October 1994.
- G.J. Marshall, R.K. Bolingbroke, and A. Gray: *Metall. Trans.*, 1993, vol. 24A, pp. 1935–42.
- G.J. Marshall, A.J.E. Flemming, A. Gray and R. Llewellyn: *Proc. 4th Int. Conf. Aluminium and Alloys*, Atlanta, USA, 1994, vol. 1, pp. 467–74.
- R. Benedictus, S.D. Meijers, A.J. Wittebrood and J.H.W. de Witt: *Proc. 6th Int. Conf. Aluminium and Alloys*, The Japan Institute of Light Metals, Toyohashi, Japan, 1998, pp. 1577–82.
- J. Liu and T. Worlitz: *NOCOLOK brazing aluminum heat exchangers*, SAE Technical Paper 950117, 1995.
- H. Jin, B. Shalchi-Amirkhiz, and D.J. Lloyd: *Metall. Mater. Trans.*, 2018, vol. 49A, pp. 1962–79.
- H. Jin: *Metall. Mater. Trans.*, 2019, vol. 50A, pp. 3868–90.
- L.F. Mondolfo: *Aluminum Alloys: Structure and Properties*, Butterworth & Co Ltd., London, UK, 1976.
- A.S. Argon: *Strengthening Mechanisms in Crystal Plasticity*, Oxford University Press, Oxford, UK, 2008.
- J.E. Hatch: *Aluminum: Properties and Physical Metallurgy*, American Society for Metals, Metals Park, 1984.
- T.W. Clyne and P.J. Withers: *An Introduction to Metal Matrix Composites*, Cambridge University Press, Cambridge, UK, 1993.
- R. Benedictus, A. Burger and A.J.P. Haszler: *US Patent 7226669B2*, June 2007.
- T. Stenqvist, K. Bång, S. Kahl, A. Contet, and O. Karlsson: *Mater. Sci. Forum*, 2014, vols. 794–796, pp. 1239–44.
- S.A. Court, K.M. Gatenby, and D.J. Lloyd: *Mater. Sci. Eng.*, 2001, vols. A319–321, pp. 443–47.
- D.J. Lloyd and S.A. Court: *Mater. Sci. Tech.*, 2003, vol. 19, pp. 1349–54.
- H. Jin: *Metall. Mater. Trans.*, 2018, vol. 49A, pp. 6122–33.
- S. Esmaili: *Precipitation hardening behaviour of AA6111*, Ph.D. Thesis, University of British Columbia, 2002.
- ASTM G69-12, *Standard Test Method for Measurement of Corrosion Potentials of Aluminum Alloys*, ASTM International, West Conshohocken, PA, 2012.
- C. Vargel: *Corrosion of Aluminium*, Elsevier Science, Amsterdam, 2004.
- M. Zamin: *Corrosion*, 1981, vol. 37, pp. 627–32.
- R.G. Buchheit: *J. Electrochemical Society*, 1995, vol. 142, pp. 3994–96.
- J.R. Davis: *ASM Specialty Handbook: Aluminium and Aluminium alloys*, ASM international, Materials Park, 1994.
- S. Fujikawa, K. Hirano, and Y. Fukushima: *Metall. Trans.*, 1978, vol. 9A, pp. 1811–15.
- J. Verlinden and R. Gijbels: *Adv. Mass. Spectrom.*, 1980, vol. 8A, pp. 485–95.
- S. Fujikawa and K. Hirano: *Def. Diff. Forum*, 1989, vols. 66–69, pp. 447–52.
- G. Rummel, T. Zumkley, M. Eggersmann, K. Freitag, and H. Mehrer: *Z. Metallkd.*, 1995, vol. 86, pp. 122–30.
- M.J. Benoit, M.A. Whitney, M.A. Wells, H. Jin, and S. Winkler: *Metall. Mater. Trans.*, 2017, vol. 48A, pp. 4645–54.

45. M.J. Benoit, R. Kaur, M.A. Wells, H. Jin, B. Shalchi-Amirkhiz, and S. Winkler: *J. Mater. Proc. Tech.*, 2018, vol. 254, pp. 353–60.
46. M.J. Benoit, H. Jin, B. Shalchi-Amirkhiz, S. Kurukuri, S. Winkler, M.J. Worswick, and M.A. Wells: *J. Mater. Proc. Tech.*, 2020, vol. 281, p. 116639.
47. H. Jin, *The role of transition metal solutes in the deformation texture, recrystallization and grain growth in aluminum and its alloys*, Ph.D. Thesis, Queen's University at Kingston, 2001.

Publisher's Note Springer Nature remains neutral with regard to jurisdictional claims in published maps and institutional affiliations.